Motion of an impurity in a two-leg ladder

Martino Stefanini,* Massimo Capone, and Alessandro Silva
International School for Advanced Studies (SISSA), Via Bonomea 265, 34136 Trieste, Italy

(Received 16 January 2021; accepted 11 March 2021; published 29 March 2021)

We study the motion of an impurity in a two-leg ladder interacting with two fermionic baths along each leg, a simple model bridging cold atom quantum simulators with an idealized description of the basic transport processes in a layered heterostructure. Using the linked-cluster expansion, we obtain exact analytical results for the single-particle Green's function and find that the long-time behavior is dominated by an intrinsic orthogonality catastrophe associated to the motion of the impurity in each one-dimensional chain. We explore both the case of two identical legs as well as the case where the legs are characterized by different interaction strengths: In the latter case, we observe a subleading correction which can be relevant for intermediate-time transport at an interface between different materials. In all the cases, we do not find significant differences between the intra- and interleg Green's functions in the long-time limit.

DOI: 10.1103/PhysRevB.103.094310

I. INTRODUCTION

The idea to design devices operating according to the laws of quantum mechanics holds the promise of a revolution where fundamental quantum phenomena can find a practical, even technological, application [1]. One of the most natural, yet very promising, perspectives in this context is the possibility to control and enhance transport properties exploiting the synergy between quantum coherence and interactions. An example of transport favored by coherence is given by molecular biocomplexes where light harvesting is particularly effective because electronic coherence survives on timescales of the order of a hundred femtoseconds [2]. Extending these ideas from molecules to solids is challenged by the fact that at the high temperatures where devices are meant to work, coherence is expected to be washed out by dephasing associated to interactions with incoherent fluctuations of the lattice, spin, and charge degrees of freedom, which are expected to act as a bath.

The fast advances in the engineering of oxide heterostructures based on a few atomic layers [3,4] can overcome these limitations, as the coherent transport through a very thin layered system can take place over timescales comparable or smaller with respect to the decoherence time [5]. This calls for theoretical investigations of the fundamental properties of few-layer interacting quantum systems. A realistic many-body calculation for an oxide heterostructure is a very demanding task, which requires advanced numerical methods able to treat strong correlations and the interaction with the excitations of the lattice. Even if the advances of numerical methods able to treat strongly correlated solids make this perspective relatively close, it is of paramount importance to reach some analytical, even if approximate, insight of the basic physical phenomena ruling the coherent transport.

In this paper, we take the latter perspective and consider the simplest system realizing, at least in principle, a very idealized version of the motion of an excitation in a layered solid, namely, an impurity in a two-leg ladder. Each leg of the ladder plays the role of a layer of the heterostructure. The hopping motion from one leg to the other will be investigated as a building block of an interlayer transport. The interaction of the impurity with gapless fermionic degrees of freedom in each leg described as Luttinger liquids is in turn the simplest possible way to describe the effect of interactions on transport. This choice also allows us to connect with well-known properties of impurity problems, including cornerstone phenomena like the Kondo effect [6] and x-ray edge singularities [7], and with quantum simulation of impurities in an ultracold atom context.

The study of the motion of impurities laso has a very long and successful history, especially focused on the conduction properties of polarons in systems with electron-lattice interactions [7]. As mentioned above, here we focus on the one-dimensional (1D) version of the problem [8–10], which allows us to introduce interactions in the Fermi system through the Tomonaga-Luttiger liquid (TLL) theory [11,12]. Moreover, the constrained geometry allows for other simplifications and theoretical techniques [10] and the existence of exact solutions [13].

The interest in the problem of 1D impurity motion has been witnessing a resurgence in the last two decades [14,15], thanks to the possibilities offered by ultracold atom techniques, which have made it possible to realize controlled and highly tunable experiments with various host interactions and impurity types [16–18]. In this perspective, the cold-atom platform also offers a framework to realize idealized versions of the phenomena ruling coherent transport in heterostructures. The 1D geometry has proven to be rich of peculiar phenomena, such as pseudo-Bloch oscillations of impurities under an external force [18] and quantum flutter in the supersonic regime [19].

*Corresponding author: martino.stefanini@sissa.it

From the theoretical point of view, an interesting discovery has been that at low momentum the polaron cannot be simply described as a quasiparticle, contrary to what happens in higher dimensions [7,20,21], which means that the effect of the bath on the impurity goes beyond the renormalization of its properties. The origin of this phenomenon lies in the orthogonality catastrophe (OC) [22] caused by the excitation of a large number of low-energy degrees of freedom within the bath.

In this paper, we characterize the Green's function of the impurity in the case in which it has access to two 1D chains connected by a tunneling term. Our main goal is to understand whether the inclusion of the discrete degree of freedom given by the presence of two chains modifies the result of the one-chain problem. We will consider the case of two identical baths and then introduce a difference in the interaction strength, mimicking interfaces between different materials in a heterostructure.

Using a linked-cluster expansion (LCE) in the interaction strength, we provide detailed calculations and analytic expressions for the Green's function, addressing the difference between the motion within each bath and the motion between the two baths and the connection with the results of a single wire. We anticipate that our results demonstrate that the motion of the impurity remains controlled by the characteristic behavior of 1D systems, suggesting that a meaningful distinction between interwire and intrawire motion requires larger systems made of several baths, eventually approaching the two-dimensional limit. The system deviates from the behavior of a single chain when the two wires are different, but this effect is subleading and it can be relevant at intermediate time before the long-time behavior is recovered.

The paper is organized as follows: in Sec. II, we introduce the model that we have used to obtain a long-wavelength description of our ladder system, and then we discuss the main results. The following Sec. III goes deeper into the LCE technique and contains more detailed results. Section III A briefly describes how the analytic results on the Green's function have been obtained. Section III B complements the previous one by illustrating a few examples of the Green's function computed numerically. Section III C shows analytic and numeric results on the impurity spectral function, while the following Sec. III D displays detailed asymptotic expressions for the single-bath case. Finally, Section IV provides some concluding remarks. Most of the technicalities are discussed in the Appendix.

II. MODEL AND MAIN RESULTS

We are interested in the investigation of the simplest process that can occur in a heterostructure: the dynamics of tunneling between two subsystems (layers in a three-dimensional heterostructure or wires in a two-dimensional one) in the presence of strong interactions within each subsystem. To focus on the essential features of this process, in the following we will consider the dynamics of a spinless impurity which can move both within any of two independent 1D wires (baths) made of interacting fermions (or bosons) or tunnel from one to the other. We make the simplifying assumption that the baths are not directly coupled with each other (our model is thus complementary to the ones analyzed in Refs. [23,24], where the baths are coupled). The Hamiltonian has the generic form

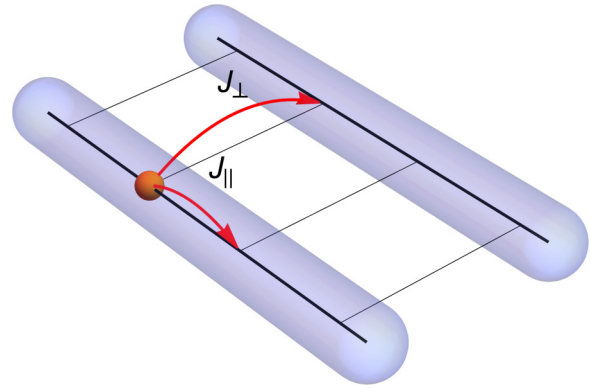

FIG. 1. The system under analysis is composed of a particle (an impurity) which is able to move through a ladder, whose legs host two independent fermion baths interacting with the impurity.

$$\mathcal{H} = \mathcal{H}_{\rm imp} + \mathcal{H}_{\rm bath} + \mathcal{H}_{\rm c}\,, \tag{1}$$

where the three terms describe the free impurity, the baths, and the impurity-bath coupling, respectively. The impurity motion can be thought of as happening on a ladder (see Fig. 1) where $J_\parallel$ and $J_\perp$ are the hopping matrix elements along and between the chains, respectively. In the present paper, we are interested in the continuum description of such a system, hence the conclusions we will reach hold irrespective of the presence of a lattice. In the long-wavelength limit the impurity dispersion is parabolic [25]:

$$\begin{aligned}\mathcal{H}_{\rm imp} = \sum_\sigma \int dx [d^\dagger_\sigma(x) E(-i\,d/dx) d_\sigma(x) \\ + -J_\perp d^\dagger_{\bar\sigma}(x) d_\sigma(x)]\,, \\ \text{with } E(p) = \frac{p^2}{2M}\,,\end{aligned} \tag{2}$$

and $M = 1/(2J_\parallel a^2)$, a being the lattice spacing. The pseudospin index $\sigma = \pm 1$ labels the two chains ($\bar\sigma = -\sigma$), and $d_\sigma(x)$ is a fermionic field (but all subsequent results equally apply to a bosonic impurity, because statistics is irrelevant for a single particle). We assume that the system is confined on a segment of length L, obeying periodic boundary conditions. At long wavelength, the baths are described by two independent TLL Hamiltonians [11],

$$\mathcal{H}_{\rm bath} = \sum_\sigma u_\sigma \int \frac{dx}{2\pi}\left[K_\sigma\left(\frac{d\theta_\sigma}{dx}\right)^2 + \frac{1}{K_\sigma}\left(\frac{d\phi_\sigma}{dx}\right)^2\right],$$

where u_σ is the sound speed in bath σ, while the Luttinger parameter K_σ measures the interaction of the particles constituting the bath. In particular, for a fermionic bath, $K_\sigma < 1$ ($K_\sigma > 1$) for repulsive (attractive) interactions. Finally, the bath-impurity coupling is chosen as the minimal one, a simple density-density interaction

$$\mathcal{H}_{\rm c} = \sum_\sigma g_\sigma \int dx\, d^\dagger_\sigma(x) d_\sigma(x) \rho_\sigma(x)\,, \tag{3}$$

with $\rho_\sigma(x)$ being the particle density of the bath σ. At the level of our treatment (long wavelength, weak coupling), this interaction can be either repulsive or attractive (i.e., $g_\sigma > 0$ or <0), as everything will only depend on g_σ^2. We will generally take $g_\sigma > 0$ for concreteness.

Bosonization [11] provides a link between density fluctuations and the boson field ϕ:

$$\rho_\sigma(x) = \rho_\sigma^{(0)} - \frac{1}{\pi}\frac{d}{dx}\phi_\sigma(x) + \rho_\sigma^{(0)} \sum_{n\neq 0} e^{2ni(\pi\rho_\sigma^{(0)}x - \phi_\sigma(x))}, \tag{4}$$

$\rho_\sigma^{(0)}$ being the average density of the bath σ. As the third term describes oscillations with large wave numbers $2n\pi\rho_\sigma^{(0)}$, we keep only the first two. The discarded terms are important only in case we want to describe fast impurities or effects like pseudo-Bloch oscillations. The constant term can be adsorbed in ϕ_σ by a canonical transformation, hence the final expression of the coupling Hamiltonian is

$$\mathcal{H}_c = -\sum_\sigma \frac{g_\sigma}{\pi}\int dx d_\sigma^\dagger(x) d_\sigma(x)\frac{d}{dx}\phi_\sigma(x). \tag{5}$$

Following Ref. [11], we express the ϕ_σ field in terms of phonon modes [26] $b_{q\sigma}$,

$$\phi_\sigma(x) = -i\pi\frac{K_\sigma^{1/2}}{L^{1/2}}\sum_{p\neq 0}\frac{V(p)}{p}e^{-ipx}(b_{p\sigma}^\dagger + b_{-p\sigma}), \tag{6}$$

and we obtain the Hamiltonian in momentum space:

$$\mathcal{H}_{\rm imp} = \sum_{p\sigma}(E(p)d_{p\sigma}^\dagger d_{p\sigma} - J_\perp d_{p\bar\sigma}^\dagger d_{p\sigma}), \tag{7a}$$

$$\mathcal{H}_{\rm bath} = \sum_{p\neq 0,\sigma} u_\sigma |p| b_{p\sigma}^\dagger b_{p\sigma}, \tag{7b}$$

$$\mathcal{H}_c = \sum_\sigma \frac{g_\sigma K_\sigma^{1/2}}{L^{1/2}}\sum_{p\neq 0} V(p) N_\sigma(p)(b_{p\sigma}^\dagger + b_{-p\sigma}). \tag{7c}$$

In the above formulas, $N_\sigma(p) = \sum_k d_{k-p,\sigma}^\dagger d_{k\sigma}$ is the Fourier transform of the impurity density and

$$V(p) = \left(\frac{|p|}{2\pi}\right)^{1/2} e^{-\alpha|p|/2},$$

where α is a small length providing an ultraviolet momentum cutoff (it can be loosely identified with the underlying lattice spacing). This cutoff is needed because the TLL description of the baths is an effective theory, valid only for small energies and momenta [7,11,12]. The choice of the shape of the cutoff function is rather arbitrary. The above one is best suited for TLL calculations. In the following, for mathematical convenience, we will switch to a cutoff in energy $\Lambda \sim 1/M\alpha^2$, rather than momentum (for more details, see Appendix A 1). Most of the relevant quantities that we will compute will be independent of the cutoff scheme.

As one can see, the role of Luttinger parameters K_σ is to rescale the bare interaction to

$$\tilde g_\sigma = g_\sigma K_\sigma^{1/2}. \tag{8}$$

This implies that baths with attractive interactions ($K_\sigma > 1$) are coupled more strongly to the impurity than baths whose particles repel each other ($K_\sigma < 1$).

We compute the impurity Green's function,

$$G_{\sigma'\sigma}(p', p; t) = -i\langle\Omega|\mathcal{T} d_{p'\sigma'}(t) d_{p\sigma}^\dagger|\Omega\rangle, \tag{9}$$

where $d_{p\sigma}(t) = e^{i\mathcal{H}t} d_{p\sigma} e^{-i\mathcal{H}t}$, $\mathcal{T}$ is the time-ordering symbol and the vector $|\Omega\rangle = |0\rangle_d|\omega\rangle_b$ is the product of the impurity vacuum $|0\rangle_d$ and the interacting bath ground state $|\omega\rangle_b$. Here $G_{\sigma'\sigma}(p', p; t)$ indeed describes the process in which we prepare the baths in their ground state $|\omega\rangle_b = \prod_\sigma |\omega_\sigma\rangle_b$ and, at time $t = 0$, we inject an impurity with a definite momentum p in the chain σ, probing the subsequent evolution by focusing on the amplitude for elastic scattering, i.e., the overlap of the state vector with every possible one-impurity state with no phonons. We notice that in ultracold atomic experiments, the return amplitude, $iG_{\sigma\sigma}(p, p; t)$, is a measurable quantity, both in real time (through interferometry) and in frequency (it gives the absorption cross section in radio-frequency spectroscopy) [27,28].

In the following, we will present a perturbative scheme to compute $G_{\sigma'\sigma}(p', p; t)$. We notice that $|\Omega\rangle$ is the ground state of the full $\mathcal{H}$ in the Hilbert space sector without impurities, i.e., $\mathcal{H}|\Omega\rangle = 0$, and it coincides with the *noninteracting* ground state within the same sector of the Hilbert space. This property, combined with the fact that the time evolution conserves the number of impurities allows us to use the Gell-Mann and Low theorem [7] to compute Eq.(9) within the standard zero-temperature perturbation theory, despite the fact that the process we are investigating is actually out of equilibrium. The perturbative series is built using $\mathcal{H}_{\rm imp} + \mathcal{H}_{\rm bath}$ as an unperturbed Hamiltonian (hence, the results will be nonperturbative in $J_\perp$), and expanding in the coupling $\tilde g_\sigma$ [29]. Because of translational invariance, it is convenient to work in momentum space and it is straightforward to see that $G_{\sigma'\sigma}(p', p; t) = \delta_{p',p} G_{\sigma'\sigma}(p, t)$ is actually diagonal in p. The detailed calculation of the Green's function is rather involved, thus we provide here the main results of our analysis.

As a benchmark, let us start our analysis with the noninteracting system. In the absence of baths, the Hamiltonian of the impurity can be easily diagonalized in terms of symmetric and antisymmetric modes $d_{p,e/o} = (d_{p,+} \pm d_{p,-})/\sqrt{2}$ with dispersion

$$\lambda_{e,o}(p) = E(p) \mp J_\perp. \tag{10}$$

The resulting Green's function is therefore the sum of two quasiparticle contributions associated to the two subbands:

$$(G_0)_{\sigma\sigma'}(p, t) = -\tfrac{i}{2}\theta(t)(e^{-i\lambda_e(p)t} + \sigma\sigma' e^{-i\lambda_o(p)t}). \tag{11}$$

In the presence of interactions within the baths, we expect two main physical effects: an OC associated to the bath response to the injection of the impurity [11,12,14,21,30] and dissipation due to the excitation of phonons in the baths. These effects can be consistently captured by a standard LCE [7,21] [31]. The outline of the derivation is presented in the following subsection. We find that, at subsonic momenta $|p| < M\min\{u_+, u_-\}$ and long times $t \gg J_\perp^{-1}, (Mu_\sigma^2)^{-1}$, the Green's function has

the asymptotic expression

$$G_{\sigma'\sigma}(p,t) \sim -\tfrac{i}{2}\left(\tfrac{t_0}{t}\right)^{\beta(p)}\left(Z_e(p,t_0)e^{-i\tilde{\lambda}_e(p)t} + \sigma'\sigma Z_o(p,t_0)e^{-2\gamma(p)t-i\tilde{\lambda}_o(p)t}\right)\left(1+O\left(\tfrac{1}{t}\right)\right), \tag{12}$$

where $\tilde{\lambda}_{e,o}(p)$ are the renormalized bands, t_0 is an arbitrary time scale and the expressions for all coefficients can be found in the Appendix. The above Green's function shows the effects mentioned before. The second factor is a renormalized version of the noninteracting Green's function. This quasiparticle behavior is spoiled by the first factor, whose power-law decay in time is the typical manifestation of the OC [7].

Being an excited state, the antisymmetric band becomes unstable, decaying exponentially with a rate $2\gamma(p)$ given by

$$2\gamma(p) = \frac{M}{8\pi}\sum_{\sigma,s=\pm1}\tilde{g}_\sigma^2\left(1-\frac{1}{\sqrt{1+2J_\perp/k_{s\sigma}(p)}}\right), \tag{13}$$

where $k_{s\sigma}(p) = (Mu_\sigma + sp)^2/2M$. Notice that for $J_\perp = 0$ this expression vanishes: This is consistent with the fact that in the absence of tunneling there cannot be emission of phonons by an impurity with subsonic speed since momentum and energy conservation cannot be simultaneously satisfied. This simple fact hinders any decay in the symmetric, low-energy band, while emission of phonons with a decay from the antisymmetric one is possible, hence the finite relaxation rate.

Interestingly, the asymmetry observed in the physics above is not present in the power-law decay associated to the OC occurring as the 1D bath rearranges in response to the injection of the impurity. The Green's function is characterized by a *single* OC exponent $\beta(p)$:

$$\beta(p) = \frac{1}{8\pi^2}\sum_\sigma \frac{g_\sigma^2 K_\sigma}{u_\sigma^2}\frac{1+(p/Mu_\sigma)^2}{(1-(p/Mu_\sigma)^2)^2}, \tag{14}$$

which is the same for all components. A comparison with Ref. [21] shows that it is proportional to the sum of the analogous single-bath exponents $\beta_\sigma^{\rm sb}(p)$ (see also Sec. III D),

$$\beta(p) = \tfrac{1}{4}(\beta_+^{\rm sb}(p) + \beta_-^{\rm sb}(p)). \tag{15}$$

Thus, this exponent is half the average of the two single-chain ones and, interestingly, it does not depend on the interchain hopping $J_\perp$. We want to stress that the above results are nonperturbative in $J_\perp$. We are led to the conclusion that the mere addition of the bath degree of freedom is able to weaken the OC but not to destroy it. To be more explicit, if the baths have identical properties, then $\beta(p) = \beta^{\rm sb}/2$.

The fact that there is only a single OC exponent characterizing both baths is related to the fact that this phenomenon is observed in the limit $J_\perp t \gg 1$, that is, when the impurity has had enough time to repeatedly interact with each bath. In fact, the numeric evaluation of the Green's function shows that for short times $J_\perp t \ll 1$ there is a dimensional crossover. At $t = 0$, $G_{\sigma\sigma}$ evolves close to the single-bath $G_\sigma^{\rm sb}$, rapidly establishing its characteristic power-law $\beta_\sigma^{\rm sb}$. Then, the impurity starts to populate the other bath and the Green's function acquires the two-bath shape.

We are inclined to think that the reason for $\beta(p)$ being less than the average of the single-bath exponents is precisely related to the fact that at weak coupling the impurity is able to spread across both baths. As a hand-waving argument, we may think that each bath effectively sees only half of the impurity, so the actual couplings become $\tilde{g}_\sigma/2$. In this picture, Eq. (15) would only state that $\beta(p)$ is the sum of the single-bath exponents computed with $\tilde{g}_\sigma/2$ instead of $\tilde{g}_\sigma$, because all of these quantities are proportional to $\tilde{g}_\sigma^2$. This line of reasoning is supported by the extension to the case of N baths, in which it would yield $\beta^N(p) = \sum_i \beta_i^{\rm sb}/N^2$. In the limit $N \to \infty$, the exponent would vanish. In such a limit, the impurity motion would become effectively two-dimensional, while the baths would still be bosonic, and so we would not get any OC.

Let us also comment on the fact that the noticeable divergence of $\beta(p)$ close to the threshold for phonon emission $p = Mu_\sigma$ is in a range of momenta were we do not expect the second-order LCE and maybe even the long-wavelength approximation to be sufficient.

From the expression Eq. (12), we can also calculate the spectral function $\hat{A}(p,\omega) \equiv -2{\rm Im}\hat{G}(p,\omega)$, finding that for $\beta(p) < 1$ (that is, for small coupling and momentum) it has a diverging threshold at $\omega = \tilde{\lambda}_e(p)$,

$$A_{\sigma\sigma}(p,\omega) \sim \theta(\omega-\tilde{\lambda}_e(p))\frac{1}{(\omega-\tilde{\lambda}_e(p))^{1-\beta(p)}}. \tag{16}$$

This is the how the power-law decay in time, hence the OC, manifests itself in the frequency domain. At higher frequency, the spectral function has a non-Lorentzian peak at the excited mode $\tilde{\lambda}_o(p)$. More details can be found in Sec. III C.

III. THE LINKED-CLUSTER EXPANSION

In single-particle problems, and especially in impurity models, the LCE [7,21] has been historically successful in providing very good approximations for the Green's function, even at intermediate coupling.

At the lowest nontrivial order, the LCE amounts to

$$\hat{G}(p,t) = \hat{G}_0(p,t)\cdot e^{\hat{F}_2(p,t)}, \tag{17}$$

where symbols with a hat will represent matrices in chain index space (σ,σ') and

$$\hat{G}_0(p,t) = -i\theta(t)\begin{pmatrix}\cos J_\perp t & i\sin J_\perp t\\ i\sin J_\perp t & \cos J_\perp t\end{pmatrix}e^{-iE_p t} \tag{18}$$

is the noninteracting impurity Green's function, $\cdot$ is the matrix product, and $\hat{F}_2(p,t)$ is defined by

$$\hat{G}_0(p,t)\cdot\hat{F}_2(p,t) = (\hat{G}_0 * \hat{\Sigma}^{(2)} * \hat{G}_0)(p,t). \tag{19}$$

In the above equation, $*$ represents a time convolution, while $\hat{\Sigma}^{(2)}(p,t)$ is the second-order self-energy [32]:

$$\hat{\Sigma}^{(2)}(p,t) = \begin{pmatrix}\Sigma_+(p,t) & 0\\ 0 & \Sigma_-(p,t)\end{pmatrix}, \tag{20}$$

where

$$\Sigma_\sigma(p,t) = ig_\sigma^2 K_\sigma\frac{1}{L}\sum_{q\neq0}V^2(q)(G_0)_{\sigma\sigma}(p-q,t)D_\sigma^0(q,t) = -i\tilde{g}_\sigma^2\theta(t)\cos J_\perp t\int\frac{dq}{2\pi}V^2(q)\,e^{-i(E(p-q)+u_\sigma|q|)t}, \tag{21}$$

with

$$D^0_\sigma(p,t) \equiv -i\langle\Omega|\mathcal{T}(b^\dagger_{p\sigma}(t)+b_{-p\sigma}(t))(b^\dagger_{-p\sigma}+b_{p\sigma})|\Omega\rangle_{\mathcal{H}_{\rm bath}}$$
$$= -i\theta(t)e^{-iu_\sigma|p|t} - i\theta(-t)e^{iu_\sigma|p|t}. \quad (22)$$

As one can see, we have chosen to work directly in the bath basis, where the physics is more transparent. In this basis, only the free impurity propagation is able to change the bath index [as $\hat{G}_0(p,t)$ is not diagonal, Eq. (18)], whereas impurity-bath interactions conserve σ.

To compute $\hat{F}_2$ from Eq. (19), it is convenient to first switch to the basis in which $\hat{G}_0(p,t)$ is diagonal. Most importantly, it is advantageous to perform the momentum integration in the self-energy Eq. (21) after the time convolution. The result of this calculation is best expressed by decomposing $\hat{F}_2$ in the matrix Pauli matrices basis $\hat{\boldsymbol{\sigma}} \equiv (\sigma_1,\sigma_2,\sigma_3)$, along with the 2×2 identity matrix $\mathbb{1}$,

$$\hat{F}_2(p,t) = A(p,t)\mathbb{1} + (B(p,t),C(p,t),D(p,t))\cdot\hat{\boldsymbol{\sigma}}\,, \quad (23)$$

where A, B, C, D are complex functions which are defined in the Appendix. The exponential is now easily computed (omitting the (p,t) arguments):

$$e^{\hat{F}_2(p,t)} = e^A\Big(\cosh\lambda\,\mathbb{1} + \frac{\sinh\lambda}{\lambda}(B,C,D)\cdot\hat{\boldsymbol{\sigma}}\Big)\,, \quad (24)$$

where

$$\lambda(p,t) \equiv \sqrt{B^2(p,t)+C^2(p,t)+D^2(p,t)} \quad (25)$$

(any of the two complex roots can be chosen).

The meaning and physical role of the above functions will become clear in the next subsection, but for now we point out that the the $C(p,t)$ and $D(p,t)$ functions are nonzero only if there is an asymmetry between the baths (in any of the u_σ, K_σ or in g_σ). The other $A(p,t)$ and $B(p,t)$ functions are less sensitive to asymmetries, and will be shown to encapsulate most of the physics of the problem.

Putting together Eqs. (24) and (18), we obtain the full expression for the Green's function:

$$G_{\sigma\sigma}(p,t) = -i\theta(t)e^{-iE(p)t+A(p,t)}$$
$$\times[\cosh\lambda\cos(J_\perp t) + i\tfrac{\sinh\lambda}{\lambda}B\sin(J_\perp t)$$
$$+\sigma\tfrac{\sinh\lambda}{\lambda}(D\cos(J_\perp t) - C\sin(J_\perp t))]\,, \quad (26a)$$
$$G_{\sigma\bar{\sigma}}(p,t) = -i\theta(t)e^{-iE(p)t+A(p,t)}$$
$$\times[i\cosh\lambda\sin(J_\perp t) + \tfrac{\sinh\lambda}{\lambda}B\cos(J_\perp t)]\,. \quad (26b)$$

This formula is rather general and thus not very enlightening but it shows that the off-diagonal elements of $\hat{G}(p,t)$ are equal, just as in the noninteracting case. This is rooted in the fact that we used the self-energy computed at second order in perturbation theory, which is diagonal in bath index space [see Eq. (20)]. Going to the next perturbative order (the fourth) allows for the inclusions of vertex corrections, which generally provide [33] $\hat{\Sigma}$ with off-diagonal elements.

In principle, given the expressions of $A(p,t)-D(p,t)$ in the Appendix, we have all the ingredients to compute the second-order LCE Green's function. In general, A, B, C, D are defined by integrals which have to be computed numerically. The results of such computations will be described in Sec. III B. However, we can obtain rather accurate asymptotic approximations at long times $t \gg (Mu_\sigma^2)^{-1}$, $J_\perp^{-1}$, as we show in the next subsection. In this way, we will understand the physical content of the Green's function that we obtained.

A. Asymptotic behavior of the Green's function

In this subsection, we build on our exact expression for $\hat{G}(p,t)$ to gain some physical insight. We will first show that its structure can be simplified and rationalized in the long-time limit, then we will display a few examples of the full numerical computation.

As stated above, we will present only results concerning subsonic impurities, for which $|p|$ is smaller than both Mu_+ and Mu_-. We are interested in this regime for two reasons: First, we do not expect our model nor the second-order LCE to be accurate when p is around Mu_σ, as the system becomes effectively strongly interacting. Second, as the threshold is exceeded, real phonons begin to be emitted in all bands and the Green's function vanishes exponentially in time thus loosing any usefulness. In fact, we have extended our calculations to this regime, finding that this happens in less than a period $2\pi/J_\perp$.

We can recast the $\hat{F}_2(p,t)$ function obtained in LCE in the following asymptotic form:

$$\hat{F}_2(p,t) \sim \hat{X}(p)t + \hat{Y}(p) + \hat{\phi}_{\rm nl}(p,t) + O\big(\tfrac{1}{t}\big)$$

for $t\to\infty$. On the right-hand side of this equation, the first two terms describe quasiparticle physics: the $\hat{X}(p)$ matrix will renormalize the single-particle properties (i.e., the mass and interbath hopping $J_\perp$) and possibly give a finite lifetime to the momentum state. The $\hat{Y}(p)$ matrix will instead quantify the (matricial) quasiparticle residue $\hat{Z} = \exp\hat{Y}$. The third term stands for any possible subleading nonlinear function of time. If any such terms are present, it causes the Green's function to depart from the quasiparticle picture. In two and three dimensions, $\hat{F}_2$ lacks any nonlinearity, and the polaron behaves as a quasiparticle [7,20]. In one dimension and with one bath, it was shown [20,21] that there is a logarithmic term, which causes the Green's function to acquire a power-law decay at long times. This is related to the OC [7,11,12,14,22,27].

In the present problem, the asymptotic expansion of F_2 can be obtained from that of A, B, C, D using Eq. (24). As shown in the Appendix, the four functions have the following asymptotic form:

$$A(p,t) \sim -\gamma(p)t - i\Delta E(p)t + c_A(p,t_0)$$
$$+ -\beta(p)\ln\tfrac{t}{t_0} + O\big(\tfrac{1}{t}\big), \quad (27a)$$
$$B(p,t) \sim \gamma(p)t + i\Delta J(p)t + c_B(p) + O\big(\tfrac{1}{t}\big), \quad (27b)$$
$$C(p,t) \sim i\frac{1-\cos 2J_\perp t}{J_\perp}c_H^{(0)}$$
$$+\frac{\sin J_\perp t}{J_\perp}\big(c_H^{(-)}e^{iJ_\perp t} - c_H^{(+)}e^{-iJ_\perp t}\big) + O\big(\tfrac{1}{t}\big), \quad (27c)$$
$$D(p,t) \sim -i\frac{\sin 2J_\perp t}{J_\perp}c_H^{(0)}$$
$$+\frac{\cos J_\perp t}{J_\perp}\big(c_H^{(+)}e^{-iJ_\perp t} - c_H^{(-)}e^{iJ_\perp t}\big) + O\big(\tfrac{1}{t}\big)\,, \quad (27d)$$

where t_0 is an arbitrary timescale, and the expressions for all the coefficients $c_{A,B}$, $c_H^{(\pm,0)}$ and ΔJ, ΔE can be found in the Appendix. We found numerically that for momenta close to zero, the approximations given above provide an excellent approximation to the Green's function for $J_\perp t \gtrsim 0.1$, i.e., for almost every relevant time. This accuracy is lost only for significantly high momenta $|p| \gtrsim 0.8Mu_\sigma$, but even in this case Eqs. (27) become reliable if t is large enough.

According to the above general considerations, the leading behavior of the $A(p,t)$ and $B(p,t)$ functions is linear in time (however, notice the logarithmic term in the former), whereas the $C(p,t)$ and $D(p,t)$ functions are purely oscillating. Therefore, at sufficiently large times, the first two are much larger than the last two, and we can approximate Eq. (25),

$$\lambda \equiv \sqrt{B^2 + C^2 + D^2} = B + O\left(\tfrac{1}{t}\right),$$

obtaining the expressions

$$G_{\sigma\sigma}(p,t) \sim -i\, e^{c_A(p)-\gamma(p)t - i\tilde{E}(p)t}(t/t_0)^{-\beta(p)} \times \cosh(c_B(p) + \gamma(p)t + i\tilde{J}_\perp(p)t)\left(1 + O\left(\tfrac{1}{t}\right)\right), \tag{28a}$$

$$G_{\sigma\bar{\sigma}}(p,t) \sim -i\, e^{c_A(p)-\gamma(p)t - i\tilde{E}(p)t}(t/t_0)^{-\beta(p)} \times \sinh(c_B(p) + \gamma(p)t + i\tilde{J}_\perp(p)t)\left(1 + O\left(\tfrac{1}{t}\right)\right), \tag{28b}$$

where

$$\tilde{E}(p) \equiv E(p) + \Delta E(p), \tag{29a}$$

$$\tilde{J}_\perp(p) \equiv J_\perp + \Delta J_\perp(p) \tag{29b}$$

are the single-particle properties modified by interactions. Notice the similarity with the noninteracting expression Eq. (18). Of course, the main difference is the already mentioned power-law decay, whose exponent has been already reported in Eq. (14).

A surprising property of Eq. (28) is that is that at late times $G_{++} \sim G_{--}(G_{+-} = G_{-+}$ is guaranteed), i.e., the effect of any difference in the baths is apparently washed out by $J_\perp$. In fact, this difference is hidden in part of the subleading $O(1/t)$ terms which have been omitted, proportional to the $C(p,t)$ and $D(p,t)$ functions.

The difference in the baths' parameters manifests itself in the functions $C(p,t)$ and $D(p,t)$ which oscillate in time, combining frequencies that are small multiples of the fundamental $J_\perp$. As will be clear in the next subsection, their contribution is essentially a high-frequency noise at small and intermediate times, which is gradually erased.

The expression Eq. (12) is recovered by simply expanding the hyperbolic functions into exponentials. We recall here its structure:

$$G_{\sigma\sigma'}(p,t) \sim -\tfrac{i}{2}\left(\tfrac{t_0}{t}\right)^{\beta(p)}\left(Z_e(p,t_0)e^{-i\tilde{\lambda}_e(p)t} + \sigma\sigma' Z_o(p,t_0)e^{-2\gamma(p)t - i\tilde{\lambda}_o(p)t}\right)\left(1 + O\left(\tfrac{1}{t}\right)\right),$$

where we introduced the complex quasiparticle weights $Z_{e,o}(p,t_0) \equiv \exp(c_A(p,t_0) \pm c_B(p))$ and the renormalized bands:

$$\tilde{\lambda}_{e,o} = \tilde{E}(p) \mp \tilde{J}_\perp(p). \tag{30}$$

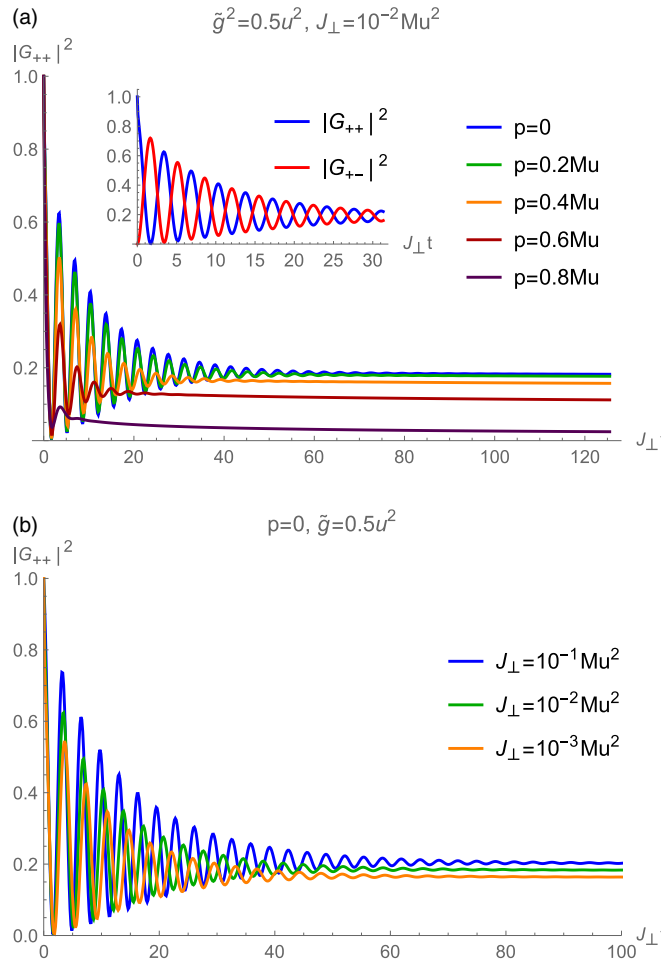

FIG. 2. Green's function for symmetric baths, obtained numerically. (a) Coherence is lost at higher p. The inset shows that G_{++} and G_{+-} have similar shapes while being out of phase. (b) Increasing $J_\perp$ causes the oscillations to live relatively longer (please notice that the time scale is $J_\perp t$). These plots allow to observe the relation between the oscillating and power-law regimes.

The contribution from the symmetric mode (which is the ground state of the system at total momentum p) decays slowly, only as a power law [34], whereas the other mode, being of higher energy, is further suppressed by an exponential decay with a characteristic time $(2\gamma(p))^{-1}$.

Up to now, we did not discuss explicitly the cutoff dependence of our results. Important measurable quantities, like $\beta(p)$ and $\gamma(p)$, are evidently independent of the high-energy properties of the baths. This does not hold for the whole Green's function. Yet Λ enters only in two terms, through $\ln\Lambda$ in both cases. The first is an irrelevant overall energy shift $\Delta E(p)$. The second dependence is within the $C(p,t)$ and $D(p,t)$ functions and their asymptotic coefficients $c_H^{(0,\pm)}$. Hence, while in the case of equal baths $G_{\sigma',\sigma}(p,t)$ is well-defined except for an overall phase factor, when the baths are different the Green's function is cutoff dependent but for very long times.

We end this section by noticing an interesting relation, valid for $J_\perp \to 0$:

$$\gamma(p) = \pi\beta(p)J_\perp + O(J_\perp^2). \tag{31}$$

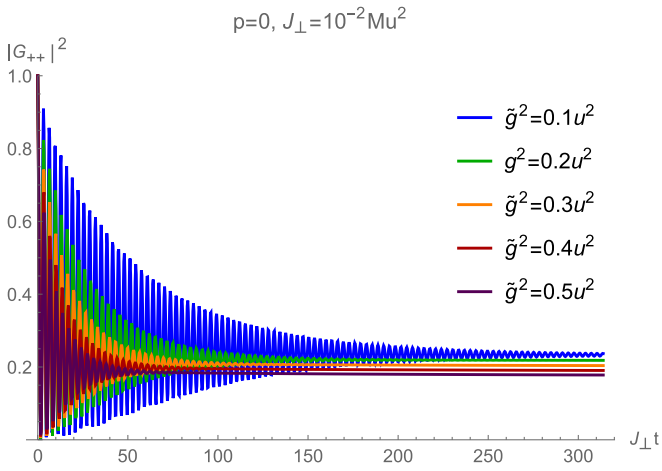

FIG. 3. Green's function for increasing strength of the impurity-bath interaction, showing how larger couplings quench the oscillations and decrease $|G|^2$.

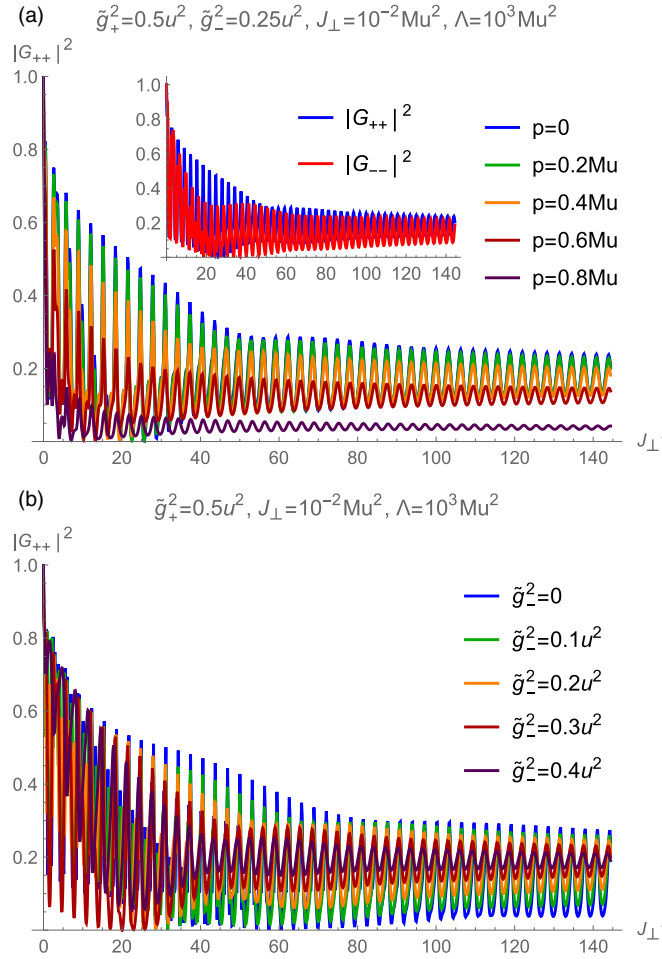

FIG. 4. Numerically obtained $|G_{++}(p,t)|^2$ when $\tilde{g}_-/u$ is lower than the fixed $\tilde{g}_+/u$. (a) The Green's function decreases faster at higher momenta. Inset: $|G_{\sigma\sigma}|^2$ is larger on the more interacting bath, although the difference decreases with time. (b) The amplitude of the oscillations increases the more different the baths are.

What makes it noteworthy is that $\gamma(p)$ is easy to compute, as it can be obtained by a straightforward Fermi's golden rule calculation, while $\beta(p)$ can be obtained only by summing infinite subdiagrams in perturbation theory (which is exactly what the LCE does).

B. Numerical results

In this subsection, we complement the analytical results reported in the previous one by showing a few plots of the full Green's function, obtained at any time by direct numerical integration of Eq. (A3) (after the simplifications explained in the Appendix).

First, the simplest case of symmetric baths is shown in Figs. 2 and 3. The general appearance of the Green's function is the following: $|G_{\sigma\sigma'}|^2$ starts oscillating (at a frequency $2\tilde{J}_\perp(p)$), with an amplitude that decays as $e^{-2\gamma(p)t}$. After a few periods, the oscillations essentially disappear, and the absolute value of both $G_\parallel \equiv G_{\sigma\sigma}$ and of $G_\perp \equiv G_{\sigma\bar{\sigma}}$ settle to the same function, which decays as the very weak power law $t^{-2\beta(p)}$. Both the diagonal $G_{++} = G_{--}$ and off-diagonal components have the same overall shape, the only difference being the fact that their oscillations are out of phase [just as in the noninteracting expression, Eq. (18)]. This is shown in the inset of Fig. 2(a).

All these features are perfectly accounted for by Eq. (12), which in fact gives an excellent approximation for all times except for $J_\perp t \lesssim 0.1$ when p is small. The oscillations are simply the result of interference of the two terms of Eq. (12), and thus they disappear after the component along the antisymmetric mode has decayed (a manifestation of decoherence).

Figures 2(a), 2(b), and 3 show how changing parameters and momentum alter the Green's function quantitatively. In general, the number of oscillations before the power-law regime decreases as p or g_σ increase or as $J_\perp$ tends to 0 (for $J_\perp = 0$ there cannot be any oscillation, obviously). This is consistent with the fact that the decay constant of the antisymmetric mode, $2\gamma(p)$, is an increasing function of p, g_σ and $J_\perp$ [see its expression in Eq. (13)]. At the same time, it can be noticed that while the number of oscillations decreases, the overall value of the Green's function also gets suppressed. This is partially caused by the increase of $\beta(p)$ for larger momentum and/or coupling.

When we break the symmetry between the baths, the situation changes rather drastically. The asymmetry can be caused by either different bath parameters u_σ, K_σ or by different couplings g_σ [35]. In our low-momentum description, g_σ and K_σ get merged into an effective coupling $\tilde{g}_\sigma$, but the actual dimensionless coupling constants are $\tilde{g}_\sigma/u_\sigma$. Therefore, we choose to vary only $\tilde{g}_\sigma$ while keeping the sound speeds constant, but the following qualitative remarks are equally valid if $u_+ \neq u_-$.

Examples of the Green's function are shown in Figs. 4 and 5. A comparison with the corresponding plots in the symmetric case shows that the overall pattern of increasing or decreasing $|G|^2$ when the parameters are varied is essentially the same. But apart from these large-scale behaviors, the plots are sharply different from the symmetric case. Most prominently, these figures generally show wider and more persisting oscillations.

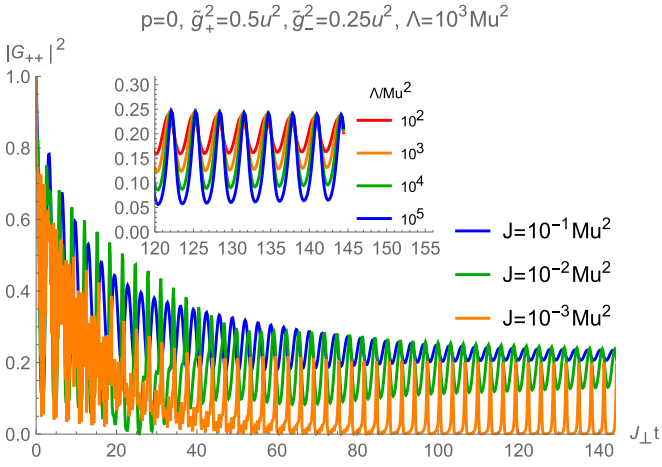

FIG. 5. Plots of the Green's function for asymmetric baths as the interchain hopping is lowered. A smaller $J_\perp$ causes $|G|^2$ to become noisier at early times and characteristically spiked at later times. The inset shows that a larger cutoff favors wider oscillations at late times.

Again, there are two different regimes, short times and longer times. The first few oscillation cycles are visibly noisy, with irregular peaks and valleys becoming whose shapes become increasingly irregular for higher momenta and (overall) couplings [Figs. 4(a) and 4(b)] and especially for the lowest $J_\perp$s (Fig. 5). We have verified that the detailed behavior in this region is strongly cutoff dependent. This suggests that it is dominated by the interference between the various terms of Eq. (26), each one depending quite sensitively from the value of Λ through the $C(p,t)$ and $D(p,t)$ functions.

As time goes on, the oscillations acquire a regular shape, with a frequency $2\tilde{J}_\perp(p)$, and a slowly decreasing amplitude. Unless we go to extremely long times, the power-law decline is explicitly seen only by looking at the average. This behavior does not appear to be related to the variation in $\gamma(p)$ as $\tilde{g}_\sigma$ are changed. In fact, if we vary the couplings in a way to keep $\gamma(p)$ fixed, we get the same results as Fig. 4(b). Moreover, this phenomenon is also rather sharp: a few percent difference between $\tilde{g}_+$ and $\tilde{g}_-$ is sufficient to observe it. Once again, its root is the UV logarithmic divergence of the $C(p,t)$ and $D(p,t)$ functions, as confirmed by varying Λ—the inset in Fig. 5 shows how a larger cutoff increases the depth of the oscillations (but leaves the maxima unchanged).

The above discussion shows that even for the large times shown the $C(p,t)$ and $D(p,t)$ functions still have a relevant influence on the Green's function, despite being asymptotically subleading. This is particularly true when $J_\perp$ is very small, as in Fig. 5. In this interesting regime, the long-term oscillations have a distinctive spiked shape, which is very far from all the other cases discussed so far. We can say that thanks to the cutoff dependence, the coherence between the symmetric and antisymmetric modes is retained longer as soon as the two baths are made unequal.

C. The spectral function

As is well known, the spectral function

$$\hat{A}(p,\omega) \equiv -2\mathrm{Im}\hat{G}(p,\omega) \tag{32}$$

yields information about the energy spectrum of the theory [7]. Moreover, we recall that it is also measurable in radio-frequency spectroscpy [28]. In our case, we can have an insight on what $\hat{A}(p,\omega)$ looks like from the asymptotic expansion, Eq. (12).

Using the fact that $\hat{G}(p,t) \propto \theta(t)$, we have

$$\begin{aligned}\hat{G}(p,\omega) &= \int_0^\infty dt e^{i\omega^+ t}\hat{G}(p,t)\\ &= \underbrace{\int_0^{\bar{t}} dt e^{i\omega^+ t}\hat{G}(p,t)}_{\hat{G}^{\mathrm{reg}}} + \underbrace{\int_{\bar{t}}^\infty dt e^{i\omega^+ t}\hat{G}(p,t)}_{\hat{G}^{\mathrm{as}}},\end{aligned}$$

where $\omega^+ = \omega + i0^+$ and $\bar{t}$ is an arbitrary time that is chosen large enough that for later times the Green's function is well approximated by the asymptotic expressions Eq. (12). Substituting these in $\hat{G}^{\mathrm{as}}$, we are left with integrals of the form

$$\int_{\bar{t}}^\infty dt \frac{e^{izt}}{t^\beta} = \frac{\Gamma(1-\beta,-iz\bar{t})}{(-iz)^{1-\beta}},$$

where

$$\Gamma(a,z) \equiv \int_z^{+\infty} dt t^{a-1}e^{-t} \tag{33}$$

is the incomplete Gamma function [36] (notice that we are interested in weak coupling and small momenta, a regime in which $\beta(p) < 1$). Putting them together, we find

$$\begin{aligned}&G^{\mathrm{as}}_{\sigma\sigma'}(p,\omega)\\ &\approx -\frac{i}{2}t_0^{\beta_p}\left[Z_e(p)\frac{\Gamma(1-\beta_p,-i(\omega^+-\tilde{\lambda}_{pe})\bar{t})}{(-i(\omega^+-\tilde{\lambda}_{pe}))^{1-\beta_p}}\right.\\ &\left.+\sigma\cdot\sigma' Z_o(p)\frac{\Gamma(1-\beta_p,-i(\omega^+-\tilde{\lambda}_{po}+2i\gamma_p)\bar{t})}{(-i(\omega^+-\tilde{\lambda}_{po}+2i\gamma_p))^{1-\beta_p}}\right],\end{aligned}$$

where most of the momentum arguments have been transformed into subscripts to improve readability.

As could have been guessed by simple scaling arguments, the power-law decay at long times corresponds to a power-law *divergence* at the frequencies of the renormalized bands [37]. On the contrary, $\hat{G}^{\mathrm{reg}}$ is an integral of a regular function over a finite domain, hence it gives a nonsingular contribution to the Green's function. Therefore, we can conclude that for frequencies around $\tilde{\lambda}_e(p)$ (and, possibly, also around $\tilde{\lambda}_o(p)$), $\hat{G}^{\mathrm{as}}$ gives the dominant contribution:

$$\begin{aligned}&G_{\sigma\sigma'}(p,\omega)\\ &\approx -\frac{i}{2}t_0^{\beta_p}\left[Z_e(p)\frac{\Gamma(1-\beta_p,-i(\omega^+-\tilde{\lambda}_{pe})\bar{t})}{(-i(\omega^+-\tilde{\lambda}_{pe}))^{1-\beta_p}}\right.\\ &\left.+\sigma\cdot\sigma' Z_o(p)\frac{\Gamma(1-\beta_p,-i(\omega^+-\tilde{\lambda}_{po}+2i\gamma_p)\bar{t})}{(-i(\omega^+-\tilde{\lambda}_{po}+2i\gamma_p))^{1-\beta_p}}\right]\\ &+\text{ regular terms for } \omega\to\tilde{\lambda}_{e,o}.\end{aligned} \tag{34}$$

When the imaginary part is taken, one observes a double-peak structure, with a thresholdlike sharper peak at $\omega = \tilde{\lambda}_e(p)$ and a broadened one around $\omega = \tilde{\lambda}_e(p)$. These are, of course, the remnants of the original noninteracting bands. This can be

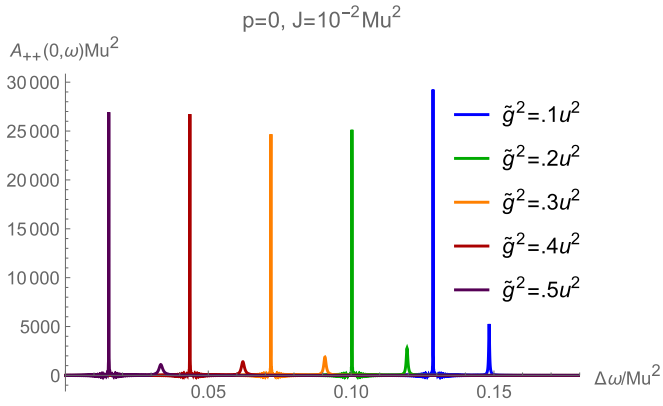

FIG. 6. Numerically computed spectral function in the symmetric case. At each coupling, the double-peak structure can be appreciated. The oscillations around the higher peaks are numerical artifacts. The frequencies are measured with respect to $\omega_0 = 1.1\tilde{\lambda}_e(p=0, \tilde{g}^2 = .5u^2)$.

appreciated clearly in Fig. 6, which shows the result of the direct numerical computation of $A_{++}(p,\omega)$.

The higher-energy peak corresponds to an unstable state and has a width of order $2\gamma(p)$, but the shape is only approximately Lorentzian. The lower energy one signals a threshold: There are no states with energies below $\tilde{\lambda}_e(p)$, while immediately above it there is an edge singularity. This can be interpreted as the impurity becoming dressed with an arbitrary number of very low-energy phonons. This edge singularity is related to the well-known x-ray threshold problem and is an established feature of impurities in 1D [7,14,21]. Analytically, it is possible to obtain

$$A_{\sigma\sigma}(p,\omega) \sim \theta(\omega-\tilde{\lambda}_e)t_0^{\beta}|Z_e(p)|\frac{\Gamma(1-\beta)\sin\beta\pi}{(\omega-\tilde{\lambda}_e(p))^{1-\beta}} \tag{35}$$

for $\omega \to \tilde{\lambda}_e^+$. This expression is remarkably similar to the spectral function of the x-ray edge problem [7].

D. Recovering the single-bath physics

In this last subsection, we make contact with the results of Refs. [21,23] for the single-bath setting. We notice that the above-mentioned works focused only on the determination of $\beta_\sigma^{\rm sb}(p)$, and all the other coefficients that we have obtained analytically for the asymptotic behavior have not been addressed.

The one-bath model is naturally recovered for $J_\perp \to 0$. However, asymptotic expressions such as Eqs. (27) are valid for $t \gg J_\perp^{-1}$, which is meaningful only if $J_\perp \neq 0$. Therefore, one should start with Eq. (A1) or simply from the definition Eq. (19). We obtain $\hat{G}(p,t) = \mathrm{diag}(G_+(p,t), G_-(p,t))$, where

$$G_\sigma(p,t) = -i\theta(t)e^{-iE(p)t+4F_\sigma(J=0,t)}, \tag{36}$$

in agreement with the calculation of Refs. [21,23]. Moreover, we have an asymptotic approximation for $F_\sigma(0,t)$ [see Eq. (A28)], which provides us with the detailed expansion

$$G_\sigma(p,t) \sim -iZ_\sigma(p,t_0)e^{i\delta_\sigma(p)}\left(\tfrac{t_0}{t}\right)^{\beta_\sigma^{\rm sb}(p)}e^{-i\tilde{E}_\sigma(p)t}\left(1+O\left(\tfrac{1}{t}\right)\right), \tag{37}$$

where

$$Z_\sigma(p,t_0) = \exp\left(-\tilde{g}_\sigma^2\frac{M}{(2\pi)^2}\sum_{s=\pm1}\frac{\ln(k_{s\sigma}t_0e^{2a_1})}{2k_{s\sigma}}\right), \tag{38a}$$

$$\delta_\sigma(p) = -\frac{\pi}{2}\beta_\sigma^{\rm sb}(p), \tag{38b}$$

$$\beta_\sigma^{\rm sb}(p) = \frac{1}{2\pi^2}\frac{g_\sigma^2K_\sigma}{u_\sigma^2}\frac{1+(p/Mu_\sigma)^2}{(1-(p/Mu_\sigma)^2)^2}, \tag{38c}$$

$$\tilde{E}_\sigma(p) = \frac{p^2}{2M}+\tilde{g}_\sigma^2\frac{M}{2\pi^2}\ln\left(\frac{2|p^2-M^2u_\sigma^2|}{M\Lambda e^{-\gamma}}\right). \tag{38d}$$

The value of the exponent $\beta_\sigma^{\rm sb}(p)$ that we found agrees with the result reported in Refs. [21,23], when expanded to second order in p/Mu_σ (except for a difference of a factor of 2 in the first momentum correction for Ref. [21]).

IV. CONCLUSIONS

In this paper, we have studied the dynamics of an impurity moving in a two-wire interacting system, a system which can be directly realized in the context of ultracold atoms and it can be considered as a minimal description of a building block of a correlated heterostructure.

Building on the results for an impurity in a single wire, Ref. [21], we have computed the impurity Green's function $\hat{G}$ using the second-order LCE. Our results are nonperturbative in the interwire hopping.

We have provided detailed analytical expressions for the leading asymptotic terms of $\hat{G}$ in the long-time limit, also complementing the results of Ref. [21], which are mainly numerical. This allowed us to obtain the renormalization of the dispersion inside the chain and of the interbath hopping, as well as the exponent of the power-law decay and the width of the antisymmetric mode.

One of our main results is that the OC, leading to the breakdown of the quasiparticle picture, survives the inclusion of a second 1D bath and dominates the long-time behavior of all the components of the Green's function.

In particular, the exponent characterizing the long-time behavior of the Green's function is given by half of the average of the exponents of the individual baths and, notably, is the same for the intrawire Green's functions and for that connecting the two wires, demonstrating that, at long times, the behavior of the system is dominated by the interactions within each wire. This implies that, for this system, the motion inside each wire and the interwire motion cannot be decoupled, suggesting that extended systems with more chains are necessary for a proper description of the transverse (with respect to the wires) motion of the impurity.

The asymptotic expansion turns out to be very accurate in comparison with a numerical evaluation of the Green's function at arbitrary times. In the case of two nonequivalent baths, the Green's function is nonuniversal, acquiring a high-frequency component at short times and exhibiting persistent oscillations at longer times. Only at asymptotically large times, the symmetric Green's function is recovered. This result may become relevant to the transport properties of heterostructures, which are built out of interfaces between

layers of a different nature, suggesting that on intermediate timescales we can observe deviation from the behavior of a single wire. Also in this case, all the components of $\hat{G}$ become asymptotically identical regardless of the interwire and intrawire character. This shows a complete decoherence between the symmetric and antisymmetric states that constitute the noninteracting eigenstates.

These results can be directly verified in the context of cold-atom quantum simulators, where the Green's functions can be directly accessed and used to build an analytical insight on more realistic models for heterostructures featuring layers instead of wires and a larger number of wires/layers.

Future work will be devoted to gain a more complete understanding of the dynamics of the system, beyond the partial information provided by the Green's function. An appealing goal would be to address the time evolution of the observables of the system and of the baths, in order to support and complement the conclusions reached in the present work. Moreover, especially in connection with the problem of coherence in heterostructures, it will be stimulating to investigate other possible parameter regimes, such as strong coupling, and settings with more than two baths.

ACKNOWLEDGMENTS

We acknowledge useful discussions with C. Giannetti. This work is supported by Italian MIUR through the PRIN2017 project CEnTral (Protocol No. 20172H2SC4).

APPENDIX: DETAILS OF THE CALCULATIONS

A. Expressions of A, B, C, D

The four components of $\hat{F}_2(p,t)$ have the expressions

$$A(p,t) = F(0,t) + \tfrac{1}{2}(F(J_\perp,t) + F(-J_\perp,t)), \tag{A1a}$$

$$B(p,t) = \tfrac{1}{2}(F(-J_\perp,t) - F(J_\perp,t)), \tag{A1b}$$

$$C(p,t) = i\frac{1-\cos 2J_\perp t}{J_\perp}H(0,t) + \frac{\sin J_\perp t}{J_\perp}[-e^{-iJ_\perp t}H(J_\perp,t) + e^{iJ_\perp t}H(-J_\perp,t)], \tag{A1c}$$

$$D(p,t) = -i\frac{\sin 2J_\perp t}{J_\perp}H(0,t) + \frac{\cos J_\perp t}{J_\perp}[e^{-iJ_\perp t}H(J_\perp,t) - e^{iJ_\perp t}H(-J_\perp,t)], \tag{A1d}$$

in terms of the functions

$$F(J,t) \equiv \sum_\sigma F_\sigma(J,t), \tag{A2a}$$

$$H(J,t) \equiv \sum_\sigma H_\sigma(J,t), \tag{A2b}$$

defined as

$$F_\sigma(J,t) \equiv -\frac{1}{4}\int_{\mathbb{R}} d\varepsilon \frac{1-i\varepsilon t - e^{-i\varepsilon t}}{\varepsilon^2} R_\sigma(\varepsilon + 2J), \tag{A3a}$$

$$H_\sigma(J,t) \equiv \sigma\frac{1}{8}\int_{\mathbb{R}} d\varepsilon \frac{1-e^{-i\varepsilon t}}{\varepsilon} R_\sigma(\varepsilon + 2J) \equiv i\frac{\sigma}{2}\frac{\partial F_\sigma(J,t)}{\partial t}, \tag{A3b}$$

for $J = \pm J_\perp$ or 0. The function $R_\sigma(\varepsilon)$ is defined as

$$R_\sigma(\varepsilon) \equiv \tilde{g}_\sigma^2 \int_{\mathbb{R}} \tfrac{dq}{2\pi} V^2(q)\delta(E(p-q) + u_\sigma|q| - E(p) - \varepsilon). \tag{A4}$$

It can be interpreted as the density of states available for scattering between the impurity and the phonons. Expressions like Eqs. (A3) and (A4) are recurrent when dealing with the OC [7,38].

Recalling that the noninteracting impurity dispersion is given by two bands $\lambda_{e,o} = E(p) \mp J_\perp$, it can be seen that for $\varepsilon \to 0$ $R_\sigma(\varepsilon)$ depends on intraband processes, while $R_\sigma(\varepsilon \pm 2J_\perp)$ give the effect of interband transitions.

Notice that all the results above hold for a generic bare impurity dispersion $E(p)$, as long as it is independent of the bath index.

Now we want to take advantage of the quadratic dispersion $E(p) = p^2/2M$, which allows us to explicitly compute $R_\sigma(\varepsilon)$. In the subsonic regime $|p| < M \max_\sigma\{u_\sigma\}$ it reads

$$R_\sigma(\varepsilon) = \tilde{g}_\sigma^2 \frac{M}{(2\pi)^2}\left[2 - \sum_{s=\pm}\frac{1}{\sqrt{1+\varepsilon/k_{s\sigma}}}\right]e^{-|\varepsilon|/\Lambda}\theta(\varepsilon), \tag{A5}$$

where

$$k_{s\sigma} \equiv \frac{(Mu_\sigma + sp)^2}{2M},\ s = \pm 1. \tag{A6}$$

In obtaining Eq. (A5), we have traded the momentum cutoff α^{-1} with an energy cutoff $\Lambda \sim 1/M\alpha^2$, which is easier to handle analytically. The low-energy physics should not be sensitive to the cutoff scheme used.

B. F_σ functions

We have to compute

$$F_\sigma(J,t) = -\frac{\tilde{g}_\sigma^2}{(4\pi)^2}\int_{-2J}^{\infty} d\varepsilon \frac{1-i\varepsilon t - e^{-i\varepsilon t}}{\varepsilon^2} e^{-|\varepsilon|/\Lambda} \times\left[2 - \sum_{s=\pm}\frac{1}{\sqrt{1+(2J+\varepsilon)/k_{s\sigma}}}\right]. \tag{A7}$$

Now we manipulate this expression to put it in a form in which it is easier to evaluate numerically, and also to extract its leading asymptotic terms at large times.

1. Case $J \neq 0$

The first part of the integral in Eq. (A7) can be calculated exactly:

$$f(J,t) \equiv 2\int_{-2J}^{\infty} d\varepsilon \frac{1-i\varepsilon t - e^{-i\varepsilon t}}{\varepsilon^2} e^{-|\varepsilon|/\Lambda}$$
$$= \pi t + 2t\,\mathrm{Si}(2Jt) - \frac{1-\cos 2Jt}{J}$$
$$+ 2it\left[\ln\frac{2|J|}{\Lambda e^{-\gamma}} + \mathrm{Re}E_1(2i|J|t) + \frac{\sin 2Jt}{2Jt}\right], \quad \text{(A8)}$$

where

$$\mathrm{Si}(z) \equiv \int_0^z dt \frac{\sin t}{t} \quad \text{(A9)}$$

is the sine integral function, and

$$E_1(z) \equiv \int_z^{\infty} dt \frac{e^{-t}}{t} \quad \text{(A10)}$$

is the exponential integral function [36]. The symbol γ denotes the Euler-Mascheroni constant. Notice that, in the above expression Eq. (A8), the limit $\Lambda \to \infty$ has been performed whenever this did not cause divergences. As can be seen, the only part which is dependent on Λ is the imaginary part of f.

When $J_\perp t \gg 1$ [39], Eq. (A8) has the asymptotic expansion (putting $J = \pm J_\perp$)

$$f(J_\perp,t) = 2\left(\pi + i\ln\frac{2J_\perp}{\Lambda e^{-\gamma}}\right)t - \frac{1}{J_\perp}$$
$$+ i\frac{e^{2iJ_\perp t}}{2J_\perp^2 t} + O\left(\frac{1}{(J_\perp t)^2}\right), \quad \text{(A11a)}$$

$$f(-J_\perp,t) = 2i\ln\frac{2J_\perp}{\Lambda e^{-\gamma}}\,t + \frac{1}{J_\perp} \quad \text{(A11b)}$$
$$+ i\frac{e^{-2iJ_\perp t}}{2J_\perp^2 t} + O\left(\frac{1}{(J_\perp t)^2}\right). \quad \text{(A11c)}$$

These expressions have been found using the expansions

$$\mathrm{Si}(z) \sim \frac{\pi}{2} - \frac{\cos z}{z} - \frac{\sin z}{z^2} + O\left(\frac{1}{z^3}\right), \quad |z| \gg 1 \quad \text{(A12a)}$$

$$E_1(z) \sim \frac{e^{-z}}{z}\left(1 - \frac{1}{z} + O\left(\frac{1}{x^2}\right)\right), \quad |z| \gg 1 \quad \text{(A12b)}$$

and the fact that $\mathrm{Si}(x)$ is odd.

The remaining integrals are in the form

$$\int_{-2J}^{\infty} d\varepsilon \frac{1-i\varepsilon t - e^{-i\varepsilon t}}{\varepsilon^2} \frac{1}{\sqrt{1+(2J+\varepsilon)/k}},$$

and are finite when the cutoff is removed. The above equation can be brought to a simpler form by doing the integral in the complex plane. The main goal is to integrate parallel to the imaginary axis, i.e., $\varepsilon \to iu$, so the integral goes from oscillatory to exponentially damped, allowing for a more efficient numerical integration. As a byproduct, some pieces of the resulting expression can be computed analytically. Moreover, this provides a shorter route to the asymptotic form when $t \to \infty$.

One first deforms the integration path as depicted in Fig. 7, from a segment on the real axis to a vertical segment followed by a quarter of circumference of radius r. This does not change the value of the integral because the only singularity of the integrand is the square root branch cut, which is chosen to lie on the real axis, to the left of $-k-2J$. Moreover, it is not difficult to see that the integral on the quarter of circumference vanishes as $1/\sqrt{r}$ when $r \to \infty$, and one obtains

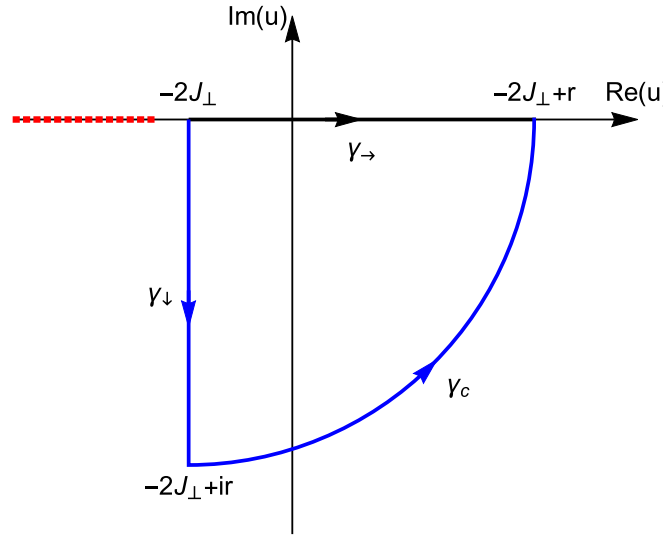

FIG. 7. Paths of integration in the complex plane. Black: Original path. Blue: Deformed path. Dotted red: Branch cut. It has been chosen to show the $J > 0$ case, the $J \leqslant 0$ ones are analogous.

$$\int_{-2J}^{\infty} d\varepsilon \frac{1-i\varepsilon t - e^{-i\varepsilon t}}{u^2} \frac{1}{\sqrt{1+(\varepsilon+2J)/k}}$$
$$= -i\int_0^{\infty} du \frac{1+i(iu+2J)t - e^{2iJt-ut}}{(iu+2J)^2} \frac{1}{\sqrt{1-iu/k}}$$
$$= -i\frac{1}{k}\phi_1(\tfrac{2J}{k}) + t\phi_2(\tfrac{2J}{k}) +$$
$$- ie^{2iJt}\int_0^{\infty} du \frac{e^{-ut}}{(iu+2J)^2}\frac{1}{\sqrt{1-iu/k}}, \quad \text{(A13)}$$

where

$$\phi_1(x) \equiv \int_0^{\infty} du \frac{1}{(iu+x)^2}\frac{1}{\sqrt{1-iu}} \quad \text{(A14a)}$$

$$\phi_2(x) \equiv \int_0^{\infty} du \frac{1}{iu+x}\frac{1}{\sqrt{1-iu}}. \quad \text{(A14b)}$$

This is the desired expression. The two functions Eqs. (A14) can be computed exactly by going back to the real axis [40],

$$\phi_1(x) = \begin{cases} \frac{1}{2x(1+x)^{3/2}}\Big[\pi x \\ \quad + -2i\left(\sqrt{x+1} + x\,\mathrm{arcsinh}(\frac{1}{\sqrt{x}})\right)\Big], & x > 0 \\ \frac{i}{|x|(1-|x|)} - \frac{i}{(1-|x|)^{3/2}}\mathrm{arccosh}(\frac{1}{\sqrt{|x|}}), & x < 0, \end{cases}$$

$$\phi_2(x) = \begin{cases} \frac{1}{\sqrt{1+x}}\left[\pi - 2i\,\mathrm{arcsinh}(\frac{1}{\sqrt{x}})\right], & x > 0 \\ -\frac{2i}{\sqrt{1-|x|}}\mathrm{arccosh}(\frac{1}{\sqrt{|x|}}), & x < 0 \end{cases} \quad \text{(A15)}$$

in which it is understood that

$$\operatorname{arccosh}(x) = i \arccos x \qquad \text{for} \quad |x| < 1.$$

The remaining integral is fast-converging when performed numerically.

When $J_\perp t \gg 1$ one can easily find an asymptotic approximation of this term, using

$$\int_a^\infty du e^{-tu} q(u) \sim e^{-at} \sum_{n=0}^{\infty} \frac{q^{(n)}(0)}{t^{n+1}}, \tag{A16}$$

when the function $q(u)$ is infinitely differentiable around $u = a$ (see Ref. [36]). This can be applied to the last integral in Eq. (A13):

$$\int_0^\infty du \frac{e^{-ut}}{(iu+2J)^2} \frac{1}{\sqrt{1-iu/k}} = \frac{1}{(2J)^2 t} + O\Big(\frac{1}{(Jt)^2}\Big).$$

Thus, the contribution of this term to the integral becomes small quite rapidly in the long-time limit.

To sum up, we can write

$$\begin{aligned}\int_{-2J}^\infty d\varepsilon \frac{1-i\varepsilon t - e^{-i\varepsilon t}}{\varepsilon^2} \frac{1}{\sqrt{1+(\varepsilon+2J)/k}} \\ = t\phi_2(\tfrac{2J}{k}) - i\frac{1}{k}\phi_1(\tfrac{2J}{k}) - i\frac{e^{2iJt}}{(2J)^2 t} + O\Big(\frac{1}{(2Jt)^2}\Big),\end{aligned} \tag{A17}$$

and putting it together with Eq. (A8), we find the sought asymptotic approximation:

$$\begin{aligned}F_\sigma(J_\perp, t) = -\tilde{g}_\sigma^2 \frac{M}{(4\pi)^2}\Bigg[-\frac{1}{J_\perp} + i\sum_{s=\pm1} \frac{1}{k_{s\sigma}} \phi_1(\tfrac{2J_\perp}{k_{s\sigma}}) \\ + \Bigg(2\pi + 2i \ln \tfrac{2J_\perp}{\Lambda e^{-\gamma}} - \sum_{s=\pm1} \phi_2\big(\tfrac{2J_\perp}{k_{s\sigma}}\big)\Bigg) t \\ + i\frac{e^{2iJ_\perp t}}{J_\perp^2 t} + O\Bigg(\frac{1}{(J_\perp t)^2}\Bigg)\Bigg],\end{aligned} \tag{A18a}$$

$$\begin{aligned}F_\sigma(-J_\perp, t) = -\tilde{g}_\sigma^2 \frac{M}{(4\pi)^2}\Bigg[\frac{1}{J_\perp} + i\sum_{s=\pm1} \frac{1}{k_{s\sigma}} \phi_1(-\tfrac{2J_\perp}{k_{s\sigma}}) \\ + \Bigg(2i \ln \tfrac{2J_\perp}{\Lambda e^{-\gamma}} - \sum_{s=\pm1} \phi_2\big(-\tfrac{2J_\perp}{k_{s\sigma}}\big)\Bigg) t \\ + i\frac{e^{-2iJ_\perp t}}{J_\perp^2 t} + O\Big(\frac{1}{(J_\perp t)^2}\Big)\Bigg].\end{aligned} \tag{A18b}$$

2. *Case $J = 0$*

Once again, the first part of Eq. (A7) is calculated exactly:

$$f(0,t) \equiv 2\int_0^\infty d\varepsilon \frac{1-i\varepsilon t - e^{-i\varepsilon t}}{\varepsilon^2} e^{-|\varepsilon|/\Lambda} = \pi t - 2it \ln \tfrac{\Lambda t}{e}. \tag{A19}$$

Already at this stage, a term proportional to $\ln t$ has appeared. The remaining integrals, which are of the form

$$\begin{aligned}\int_0^\infty d\varepsilon \frac{1+i\varepsilon t - e^{-i\varepsilon t}}{\varepsilon^2} \frac{1}{\sqrt{1+\varepsilon/k}} \\ = i\int_0^\infty du \frac{1-ut-e^{-ut}}{u^2} \frac{1}{\sqrt{1-iu/k}},\end{aligned} \tag{A20}$$

cannot be separated into three components as in the $J_\perp \neq 0$ case, because the kernel $(1-ut-e^{-ut})/u^2$ has to be treated carefully at the $u = 0$ integration limit. One can do the following:

$$\begin{aligned}\int_0^\infty d\varepsilon \frac{1-i\varepsilon t - e^{-i\varepsilon t}}{\varepsilon^2} \frac{1}{\sqrt{1+\varepsilon/k}} \\ = t\Bigg[\underbrace{\int_0^{\bar\varepsilon} d\varepsilon \frac{1-i\varepsilon - e^{-i\varepsilon}}{\varepsilon^2} \frac{1}{\sqrt{1+\varepsilon/\bar\varepsilon}}}_{I} \\ + \underbrace{\int_{\bar\varepsilon}^\infty d\varepsilon \frac{1-i\varepsilon - e^{-i\varepsilon}}{\varepsilon^2} \frac{1}{\sqrt{1+\varepsilon/\bar\varepsilon}}}_{II}\Bigg],\end{aligned} \tag{A21}$$

with the substitution $\varepsilon \to \varepsilon/t$ and using the notation $\bar\varepsilon \equiv kt$. The first integral can be estimated for large t, i.e., for large $\bar\varepsilon$, by expanding the square root in powers of $\varepsilon/\bar\varepsilon$:

$$\begin{aligned}I \sim \sum_{n=0}^\infty \binom{-1/2}{n} \frac{1}{\bar\varepsilon^n} \int_0^{\bar\varepsilon} d\varepsilon \frac{1-i\varepsilon - e^{-i\varepsilon}}{\varepsilon^2} \varepsilon^n \\ = \frac{\pi}{2} - \Big(1 + \frac{\gamma}{2} - c_1\Big)\frac{1}{\bar\varepsilon} - \frac{\ln\bar\varepsilon}{\bar\varepsilon} \\ + i\Big(1 - \gamma - c_0 - \ln\bar\varepsilon - \frac{\pi}{4\bar\varepsilon}\Big) + O\big(\tfrac{1}{\bar\varepsilon^2}\big),\end{aligned} \tag{A22}$$

where

$$c_0 \equiv \sum_{n\geqslant 1} \binom{-1/2}{n} \frac{1}{n} = \ln 4 - 2\operatorname{arcsinh}(1), \tag{A23a}$$

$$\begin{aligned}c_1 &\equiv \sum_{n\geqslant 2} \binom{-1/2}{n} \frac{1}{n-1} \\ &= \frac{3-2\sqrt{2}}{2} - \ln 2 + \operatorname{arcsinh}(1).\end{aligned} \tag{A23b}$$

To obtain these results, we integrated explicitly all terms in the series and expanded them up to $O(\bar\varepsilon^{-2})$. As one can see, terms containing $\ln t$ have appeared. These are due to the structure of the kernel $(1-i\varepsilon-e^{-i\varepsilon})/\varepsilon^2$ for $\varepsilon \sim 0$.

The second integral avoids the neighborhood of $\varepsilon = 0$ and therefore it can be computed straightforwardly:

$$\begin{aligned}II = \underbrace{\int_{\bar\varepsilon}^\infty d\varepsilon \frac{1}{\varepsilon^2\sqrt{1+\varepsilon/\bar\varepsilon}}}_{II_a} \\ + \underbrace{-i\int_{\bar\varepsilon}^\infty d\varepsilon \frac{1}{\varepsilon\sqrt{1+\varepsilon/\bar\varepsilon}}}_{II_b} \underbrace{-\int_{\bar\varepsilon}^\infty d\varepsilon \frac{e^{-i\varepsilon}}{\varepsilon^2\sqrt{1+\varepsilon/\bar\varepsilon}}}_{II_c},\end{aligned} \tag{A24}$$

giving

$$II_a = \frac{1}{\bar\varepsilon}\int_1^\infty d\varepsilon \frac{1}{\varepsilon^2\sqrt{1+\varepsilon}} = \frac{\sqrt{2}-\operatorname{arcsinh}(1)}{\bar\varepsilon},$$
$$II_b = -i\int_1^\infty d\varepsilon \frac{1}{\varepsilon\sqrt{1+\varepsilon}} = -2i\operatorname{arcsinh}(1),$$
$$II_c = -\int_{\bar\varepsilon}^\infty d\varepsilon \frac{e^{-i\varepsilon}}{\varepsilon^2\sqrt{1+\varepsilon/\bar\varepsilon}} \sim \frac{ie^{-i\bar\varepsilon}}{\sqrt{2}\bar\varepsilon^2} + O\left(\tfrac{1}{\bar\varepsilon^3}\right),\ \bar\varepsilon \gg 1,$$

where for the last estimate we used the analogous of Eq. (A16) [36]:

$$\int_a^\infty d\varepsilon e^{ix\varepsilon} q(\varepsilon) \sim e^{iax}\sum_{n=0}^\infty q^{(n)}(a)\left(\tfrac{i}{x}\right)^{n+1} \quad x \gg 1. \tag{A25}$$

Hence,

$$II \sim -2i\operatorname{arcsinh}(1) + \frac{\sqrt{2}-\operatorname{arcsinh}(1)}{\bar\varepsilon} + \frac{ie^{-i\bar\varepsilon}}{\sqrt{2}\bar\varepsilon^2} + O\left(\tfrac{1}{\bar\varepsilon^3}\right),$$

which, unlike the I integral, does not contain any term depending logarithmically on $\bar\varepsilon$.

The final estimate is

$$\int_0^\infty d\varepsilon \frac{1+i\varepsilon t - e^{i\varepsilon t}}{\varepsilon^2}\frac{1}{\sqrt{1+\varepsilon/k}}$$
$$= t(I+II) = -\frac{a_1}{k} - \frac{\ln kt}{2k} + \frac{\pi}{2}t$$
$$+ i\left[-\frac{\pi}{4k} - t\ln kt + (1-\gamma-\ln 4)t\right] + O\left(\tfrac{1}{t}\right), \tag{A26}$$

where

$$a_1 \equiv \ln 2 - \frac{1-\gamma}{2}. \tag{A27}$$

Putting all terms together, we obtain the asymptotic approximation

$$F_\sigma(0,t) \sim -\tilde g_\sigma^2 \frac{M}{(4\pi)^2}\left[\left(2a_1 + i\frac{\pi}{2}\right)\sum_{s=\pm1}\frac{M}{(p+sMu_\sigma)^2}\right.$$
$$+ \sum_{s=\pm1}\frac{M}{(p+sMu_\sigma)^2}\ln\frac{(p+sMu_\sigma)^2 t}{2M}$$
$$\left. + 2it\ln\frac{2|p^2-M^2u_\sigma^2|}{M\Lambda e^{-\gamma}} + O\left(\tfrac{2M}{(p\pm Mu_\sigma)^2 t}\right)\right],$$
$$\text{for}\quad \frac{(p\pm Mu_\sigma)^2 t}{2M} \gg 1. \tag{A28}$$

C. H_σ functions

The H_σ functions are obtained from the F_σ ones by

$$H_\sigma(J,t) = i\frac{\sigma}{2}\frac{\partial F_\sigma(J,t)}{\partial t}.$$

The fast-converging integral expression is

$$H_\sigma(J,t) = \sigma\frac{\tilde g_\sigma^2 M}{2(4\pi)^2}\left[h(J,t) + i\sum_{s=\pm1}\left(\phi_2\left(\tfrac{2J}{k_{s\sigma}}\right)\right.\right.$$
$$\left.\left. + -\int_0^\infty d\varepsilon \frac{e^{2iJt-t\varepsilon}}{i\varepsilon+2J}\frac{1}{\sqrt{1-i\varepsilon/k_{s\sigma}}}\right)\right], \tag{A29}$$

where

$$h(\pm J_\perp, t) = 2\ln\tfrac{2J_\perp}{\Lambda e^{-\gamma}} + 2\mathrm{Re}E_1(2iJ_\perp t)$$
$$+ -i\left(\pi \pm 2\mathrm{Si}(2J_\perp t)\right)$$
$$\sim 2\ln\tfrac{2J_\perp}{\Lambda e^{-\gamma}} - i(1\pm1)\pi$$
$$\pm i\frac{e^{\pm 2iJ_\perp t}}{J_\perp t} + O\left(\tfrac{1}{(J_\perp t)^2}\right), \tag{A30a}$$
$$h(0,t) = -2\ln\Lambda t - i\pi. \tag{A30b}$$

The asymptotic expansions are

$$H_\sigma(J_\perp,t) = \sigma\frac{\tilde g_\sigma^2 M}{2(4\pi)^2}\left(2\ln\tfrac{2J_\perp}{\Lambda e^{-\gamma}} - 2i\pi\right.$$
$$\left. + i\sum_{s=\pm1}\phi_2\left(\tfrac{2J_\perp}{k_{s\sigma}}\right) - 2i\frac{e^{2iJ_\perp t}}{J_\perp t} + O\left(\tfrac{1}{(J_\perp t)^2}\right)\right), \tag{A31a}$$

$$H_\sigma(-J_\perp,t) = \sigma\frac{\tilde g_\sigma^2 M}{2(4\pi)^2}\left(2\ln\tfrac{2J_\perp}{\Lambda e^{-\gamma}}\right.$$
$$\left. + i\sum_{s=\pm1}\phi_2\left(-\tfrac{2J_\perp}{k_{s\sigma}}\right) + 2i\frac{e^{-2iJ_\perp t}}{J_\perp t} + O\left(\tfrac{1}{(J_\perp t)^2}\right)\right), \tag{A31b}$$

$$H_\sigma(0,t) = \sigma\frac{\tilde g_\sigma^2 M}{2(4\pi)^2}\left(2\ln\tfrac{2|p^2-M^2u_\sigma^2|}{M\Lambda e^{-\gamma}}\right.$$
$$\left. + - i\sum_{s=\pm1}\frac{1}{2k_{s\sigma}t} + O\left(\tfrac{1}{(J_\perp t)^2}\right)\right). \tag{A31c}$$

As one can see, all these functions tend to a constant at $t\to\infty$ (as they should, being derivatives of asymptotically linear functions F_σ).

D. Asymptotic expansion of A, B, C, D

Above, we found the necessary ingredients to compute the leading asymptotic behavior of the $\hat F_2(p,t)$ function. The result is Eqs. (27), with the coefficients given by

$$\beta(p) = \frac{M}{2(4\pi)^2}\sum_{s,\sigma}\frac{\tilde g_\sigma^2}{k_{s\sigma}}, \tag{A32a}$$

$$\gamma(p) = \frac{M}{32\pi}\sum_{\sigma,s}\tilde g_\sigma^2\left(1 - \frac{1}{\sqrt{1+2J_\perp/k_{s\sigma}}}\right), \tag{A32b}$$

$$c_A(p,t_0) = -\frac{M}{2(4\pi)^2}\sum_{s,\sigma}\frac{\tilde g_\sigma^2}{k_{s\sigma}}\left[2a_1 + \ln k_{s\sigma}t_0\right.$$
$$\left. + i\left(\phi_1\left(\tfrac{2J_\perp}{k_{s\sigma}}\right) + \phi_1\left(-\tfrac{2J_\perp}{k_{s\sigma}}\right) + \tfrac{\pi}{2}\right)\right], \tag{A32c}$$

$$c_B(p) = -\frac{M}{2(4\pi)^2}\sum_{s,\sigma}\frac{\tilde{g}_\sigma^2}{k_{s\sigma}}\left[\frac{k_{s\sigma}}{J_\perp} + i\left(\phi_1\left(\tfrac{-2J_\perp}{k_{s\sigma}}\right) - \phi_1\left(\tfrac{2J_\perp}{k_{s\sigma}}\right)\right)\right], \tag{A32d}$$

$$\Delta E(p) = \frac{M}{(4\pi)^2}\sum_{s,\sigma}\tilde{g}_\sigma^2\left[\ln\left(\tfrac{4J_\perp}{\Lambda e^{-\gamma}}\tfrac{|p^2-M^2u_\sigma^2|}{M\Lambda e^{-\gamma}}\right) + \tfrac{\operatorname{arcsinh}(\sqrt{k_{s\sigma}/2J_\perp})}{\sqrt{1+2J_\perp/k_{s\sigma}}} + \tfrac{\operatorname{arccosh}(\sqrt{k_{s\sigma}/2J_\perp})}{\sqrt{1-2J_\perp/k_{s\sigma}}}\right], \tag{A32e}$$

$$\Delta J(p) = -\frac{M}{(4\pi)^2}\sum_{s,\sigma}\tilde{g}_\sigma^2\left[\tfrac{\operatorname{arccosh}(\sqrt{k_{s\sigma}/2J_\perp})}{\sqrt{1-2J_\perp/k_{s\sigma}}} + -\tfrac{\operatorname{arcsinh}(\sqrt{k_{s\sigma}/2J_\perp})}{\sqrt{1+2J_\perp/k_{s\sigma}}}\right], \tag{A32f}$$

and

$$c_H^{(+)}(p) = \frac{M}{2(4\pi)^2}\sum_{s,\sigma}\sigma\tilde{g}_\sigma^2\left(\ln\tfrac{2J_\perp}{\Lambda e^{-\gamma}} - i\pi + i\phi_2\left(\tfrac{2J_\perp}{k_{s\sigma}}\right)\right), \tag{A33a}$$

$$c_H^{(-)}(p) = \frac{M}{2(4\pi)^2}\sum_{s,\sigma}\sigma\tilde{g}_\sigma^2\left(\ln\tfrac{2J_\perp}{\Lambda e^{-\gamma}} + i\phi_2\left(-\tfrac{2J_\perp}{k_{s\sigma}}\right)\right), \tag{A33b}$$

$$c_H^{(0)}(p) = \frac{M}{(4\pi)^2}\sum_{\sigma}\sigma\tilde{g}_\sigma^2\ln\tfrac{2\left|p^2-M^2u_\sigma^2\right|}{M\Lambda e^{-\gamma}}, \tag{A33c}$$

where t_0 is an arbitrary time scale (so that the physical dimensions are consistent).

One should note that only $\Delta E(p)$ and the three $c_H(p)$s bear a (logarithmic) dependence on the cutoff Λ. The former is an energy shift, so it is reasonable that it depends sensitively on the behavior of the theory at high energy. Conversely, measurable quantities like $\tilde{J}_\perp \equiv J_\perp + \Delta J$ and $\beta(p)$ are cutoff independent and thus proper low-energy properties.

We would also like to make some remarks about the region of validity of the asymptotic expansions presented in this paper. We have found that, numerically, the expressions Eqs. (27) give rather accurate results even for times $J_\perp t \sim 0.1$, at least for $|\hat{G}(p,t)|$ and $p \lesssim 0.8\,Mu$. Increasing the momentum causes one of the $k_{s\sigma}(p)$ to become small, and hence the asymptotic expressions retain their reliability only at larger times. This is also valid for the approximation given in Eqs. (28) or (12) in the case of symmetric baths. For increasing asymmetry, Eqs. (28) and (12) are reliable only for larger times, depending on the parameters used.

[1] S. Huelga and M. Plenio, Contemp. Phys. **54**, 181 (2013).
[2] G. D. Scholes, G. R. Fleming, A. Olaya-Castro, and R. van Grondelle, Nat. Chem. **3**, 763 (2011).
[3] P. Zubko, S. Gariglio, M. Gabay, P. Ghosez, and J.-M. Triscone, Annu. Rev. Condens. Matter Phys. **2**, 141 (2011).
[4] H. Y. Hwang, Y. Iwasa, M. Kawasaki, B. Keimer, N. Nagaosa, and Y. Tokura, Nat. Mater. **11**, 103 (2012).
[5] C. M. Kropf, A. Valli, P. Franceschini, G. L. Celardo, M. Capone, C. Giannetti, and F. Borgonovi, Phys. Rev. B **100**, 035126 (2019).
[6] J. Kondo, Prog. Theor. Phys. **32**, 37 (1964).
[7] G. D. Mahan, *Many-Particle Physics*, 2nd ed. (Plenum Press, New York, 1993).
[8] A. H. Castro Neto and A. O. Caldeira, Phys. Rev. Lett. **67**, 1960 (1991).
[9] T. Ogawa, A. Furusaki, and N. Nagaosa, Phys. Rev. Lett. **68**, 3638 (1992).
[10] A. H. Castro Neto and A. O. Caldeira, Phys. Rev. B **46**, 8858 (1992).
[11] T. Giamarchi, *Quantum Physics in One Dimension*, 1st ed. (Clarendon Press, Oxford, 2003).
[12] A. O. Gogolin, A. A. Nersesyan, and A. M. Tsvelik, *Bosonization and Strongly Correlated Systems* (Cambridge University Press, Cambridge, 1998).
[13] J. B. McGuire, J. Math. Phys. **6**, 432 (1965).
[14] A. Lamacraft, Phys. Rev. B **79**, 241105(R) (2009).
[15] M. Schecter, D. Gangardt, and A. Kamenev, Ann. Phys. **327**, 639 (2012).
[16] S. Palzer, C. Zipkes, C. Sias, and M. Köhl, Phys. Rev. Lett. **103**, 150601 (2009).
[17] J. Catani, G. Lamporesi, D. Naik, M. Gring, M. Inguscio, F. Minardi, A. Kantian, and T. Giamarchi, Phys. Rev. A **85**, 023623 (2012).
[18] F. Meinert, M. Knap, E. Kirilov, K. Jag-Lauber, M. B. Zvonarev, E. Demler, and H.-C. Nägerl, Science **356**, 945 (2017).
[19] C. J. M. Mathy, M. B. Zvonarev, and E. Demler, Nat. Phys. **8**, 881 (2012).
[20] A. Rosch, Adv. Phys. **48**, 295 (1999).
[21] A. Kantian, U. Schollwöck, and T. Giamarchi, Phys. Rev. Lett. **113**, 070601 (2014).
[22] P. W. Anderson, Phys. Rev. Lett. **18**, 1049 (1967).
[23] N. A. Kamar, A. Kantian, and T. Giamarchi, Phys. Rev. A **100**, 023614 (2019).
[24] N. A Kamar, Quantum dynamics in one-dimensional and two-leg ladder systems, Ph.D. thesis, University of Geneva, 2019.
[25] We use units such that $\hbar = 1$.
[26] We are implicitly dropping terms of $O(1/L)$, that give vanishing contributions in the thermodynamic limit.
[27] M. Knap, A. Shashi, Y. Nishida, A. Imambekov, D. A. Abanin, and E. Demler, Phys. Rev. X **2**, 041020 (2012).
[28] A. Shashi, F. Grusdt, D. A. Abanin, and E. Demler, Phys. Rev. A **89**, 053617 (2014).
[29] It can be easily seen that g_σ has the dimension of a speed, so that the dimensionless coupling constant is actually $\tilde{g}_\sigma/u_\sigma$. Compare with the expression for $\beta(p)$ (Eq.(14)).
[30] A. Rosch and T. Kopp, Phys. Rev. Lett. **75**, 1988 (1995).
[31] In Ref. [24] online an analogous calculation is performed in a generalization of the model we are studying, with the

complication that also the fermions constituting the baths can hop between the legs of the ladder.

[32] Within our model, there is no tadpole contribution, because $\hat{G}_0(p, 0^-) = 0$ and because there are no zero-momentum phonons.

[33] However, this may not happen if $\tilde{g}_+ \neq \tilde{g}_-$ but the sound speeds u_σ are the same.

[34] Notice that for momenta $p \ll M u_\sigma$ and small coupling $\tilde{g}_\sigma / u_\sigma < 1$, $\beta(p)$ is a small number of the order of 10^{-2}.

[35] Strictly speaking, one could also allow for different cutoffs Λ_σ. We preferred to avoid this complication.

[36] DLMF, NIST Digital Library of Mathematical Functions, release 1.0.25 of Dec. 15, 2019, edited by f. W. J. Olver, A. B. Olde Daalhuis, D. W. Lozier, B. I. Schneider, R. F. Boisvert, C. W. Clark, B. R. Miller, B. V. Saunders, H. S. Cohl, and M. A. McClain, http://dlmf.nist.gov/.

[37] $\Gamma(a, z) = \Gamma(a) + O(z)$ for $z \to 0$, so it does not change the singular behavior as long as $a \neq 1$, i.e., $\beta(p) \neq 1$. For $\beta(p) = 1$, one has a logarithmic divergence.

[38] K. D. Schotte and U. Schotte, Phys. Rev. **182**, 479 (1969).

[39] Usually, we expect $J_\perp \ll k \sim M u_\sigma^2/2$, i.e., the interbath tunneling amplitude to be far smaller than the intrabath one.

[40] One may exploit the observation that $\phi_1(x) = -\frac{d\phi_2}{dx}$.